ISTITUTO NAZIONALE DI RICERCA METROLOGICA
Repository Istituzionale

Stable Frequency References in the Optical Domain for Aerospace Applications - Part I - Preliminary Considerations on Cavity Design and Thermal Stabilization

(Article begins on next page)

02 May 2024

Stable Frequency References in the Optical Domain for Aerospace Applications

Part I
Preliminary Considerations on Cavity Design and Thermal Stabilization

M. Bisi and C. Francese

Istituto Nazionale di Ricerca Metrologica,
Strada delle Cacce 91, 10135 Torino, ITALY

E-mail: `m.bisi@inrim.it`, `c.francese@inrim.it`

Abstract. We report on the development of an optical cavity at $\lambda = 1064$ nm to be used as a frequency reference in aerospace applications.

INRIM Technical Report 3/2010

1. Introduction

Long term frequency stability of lasers is a key parameter in many research areas ranging from dimensional metrology to fundamental physics. Many solutions have been proposed by the scientific community and lasers whose frequency is referenced to molecular transitions are commonly used when long term stability and wavelength accuracy are needed.

This report describes the design of an high-finesse optical cavity to be used as a reference for laser frequency stabilization.
High finesse cavities have been widely studied (and used) in many application: the novelty of our work is the use of the cavity on board of a spacecraft. Given the particular application, the cavity must be compliant with the huge acceleration experienced during the launch phase (up to 30g at 1 kHz).
A pecularity of our realization is that, contrary to the normal practice, the cavity is used as a long-term reference (over a one-day time scale typically). Since the resonant frequency depends on the cavity length, it is necessary to control the environment in order to avoid mechanical and thermal disturbances which can possibly lead to a variation of the cavity length.

Our goal is the development of a frequency stabilization system with a relative frequency stability (Allan variance) of 10^{-12} over 1 second integration time which will be suitable for aerospace applications. The frequency reference is a 10 cm long Fabry-Perot optical resonator which has been designed in order to withstand the launch loads. As the stability of the resonant frequency is determined by the long term stability of the cavity length, a low CTE material (ULE) was adopted as the cavity spacer.
The cavity itself is nothing without a control loop which detects the detuning of the laser frequency with respect to the frequency of the cavity and generates an error signal which is fed back to the laser frequency actuator(s). The adopted stabilization scheme is the Pound-Drever method [1]. The elements constituting the control loop are a phase modulator (EOM), a detector (photodiode), a demodulator and a loop filter, as shown in Figure 1.
The mechanical design of the cavity and its enclosure is covered by [2], while the cavity thermal control is addressed in [3].

This document focuses on the mechanical and optical design of the cavity and on the cavity thermal model.
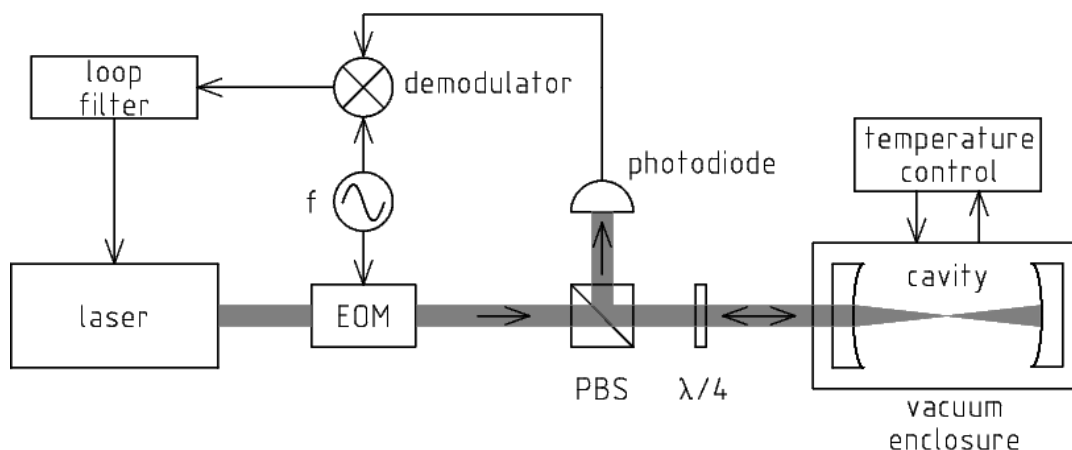
Figure 1. Frequency stable laser block scheme
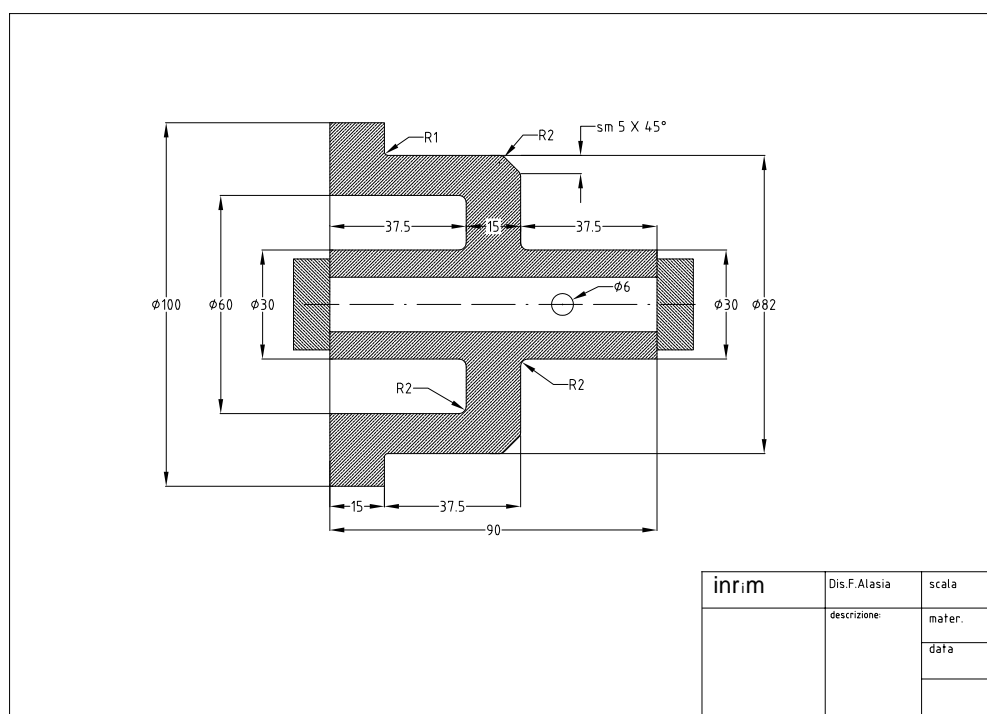
Figure 2. Cavity spacer

2. Cavity assemby

The cavity is constituted by a 90 mm long ULE spacer and two high-reflectivity curved mirrors contacted at the spacer ends, as seen in Figure 2.

Because of the acceleration experienced during the launch, the usual optical contact seems not adequate for contacting the mirrors to the ULE spacer. The hydroxy-catalysis bonding could be used instead. Since prototyping costs are a driving parameter, the actual bonding technique will be defined at a later stage.

Table 1. Physical properties and figure of merit of optical glasses

Material	Density	Young modulus	Poisson ratio	Knoop hardness	Specific stiffness
	g cm^{-3}	GPa		kg mm^{-2}	N m g^{-1}
Zerodur EC0	2.53	91	0.24	630	3.6 $\times 10^3$
ULE	2.21	67.6	0.17	460	3.1 $\times 10^3$

Table 2. Thermal properties and figure of merit of optical glasses

Material	Zerodur EC0	ULE	
CTE	0.021	0.0 ± 0.03	$\times 10^{-6}$K^{-1}
Thermal conductivity @ 300 K	1.64	1.31	W m^{-1} K^{-1}
Specific heat	821	776	J kg K
Thermal diffusivity	0.8	0.8	$\times 10^{-6}$ m^2 s^{-1}
Steady-state thermal distorsion	0.01	< 0.02	$\times 10^{-6}$ m W^{-1}
Transient thermal distorsion	0.03	< 0.04	s m^{-2} K^{-1}
Thermal stress	901	> 646	$\times 10^{-6}$ m N^{-1}

With the hydroxy-catalysis, a very thin bond (80-100 nm) is formed, giving a bond strength comparable with that of the bulk (actually, it seems that the bond strength is 20 times less than the bulk [4]) and a good resistance to large temperature fluctuations (from cryogenic to 800 °C) [5]. The hydroxy-catalysis bonding has been successfully tested for its reliability under vibration and thermal cycling [4], [6].

Table 1 shows the mechanical properties of some optical glasses; Table 2 shows the thermal properties of some optical glass [7], [8].

Figure 3 shows the cavity mirrors design. The surfaces to be contacted must have a flatness of about $\lambda/10$ and must have a cleaness compatible to that of a Class 10 clean room; in order to ensure a proper bonding, the uncoated surface must be flat [9]. According to the mirror manufacturer, it is not possible to mask the mirror in such a way that the flat surface will not be deposited; after the deposition, the flat surface will be carefuly polished to the level specified, and than the usual Si0$_2$ protective layer (which is compatible with the hydroxy-catalysis bonding) will be deposited [10].

2.1. Mirror reflectivity

The target cavity finesse is 10 000: from Figure 4, it is seen that such a finesse is obtained for (equal) mirror reflectivities R=99.9686%. The mirror reflectivities available from the manufacturer are $(99.8 \pm 0.05)\%$, $(99.95 \pm 0.02)\%$ and $(99.98 \pm 0.005)\%$. Table 3 shows the finesse obtainable from the given nominal refectivities. We are forced to choose a mirror reflectivity which gives a finesse higher than the desired one.
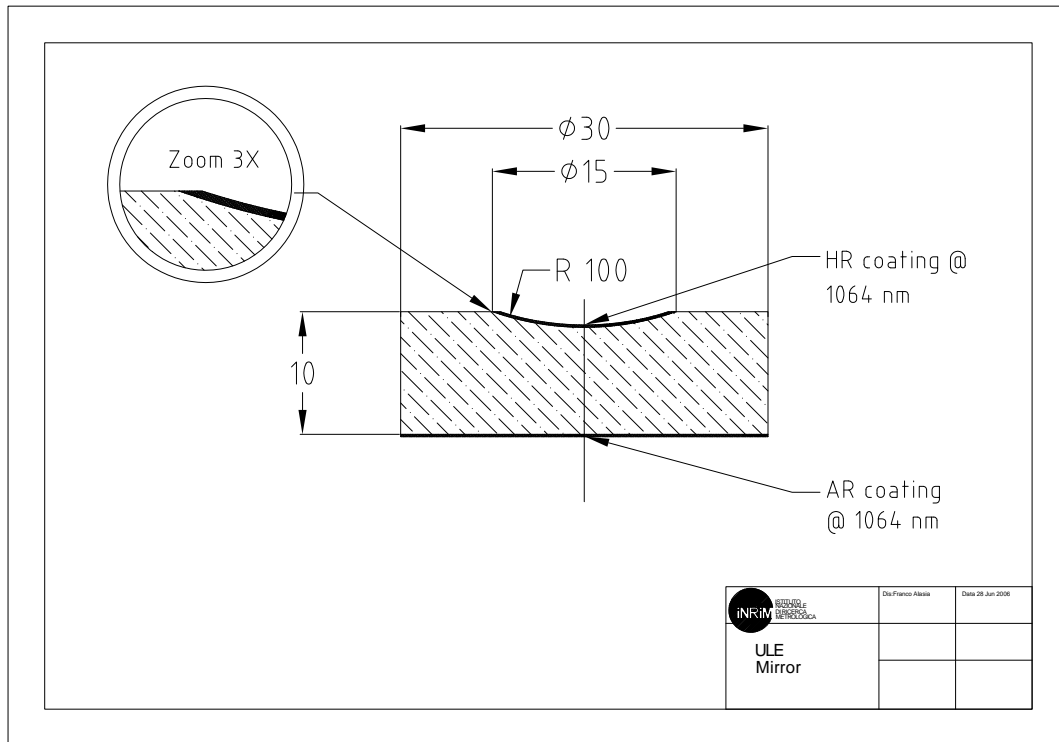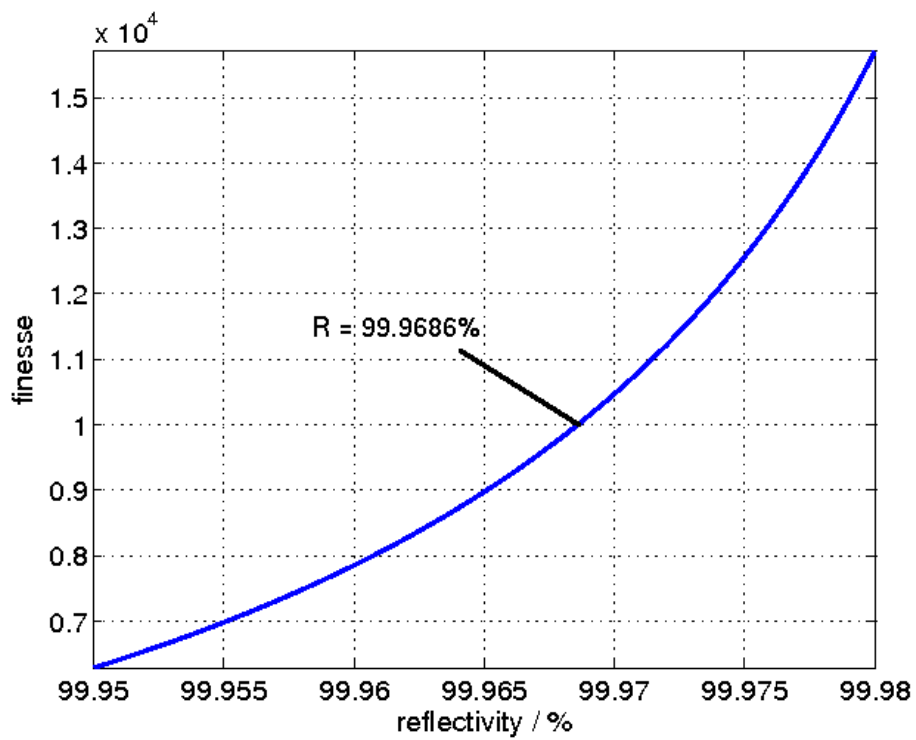
Figure 3. Cavity mirror

Figure 4. Cavity finesse as a function of mirror reflectivity

Table 3. Cavity finesse for the various manufacturer reflectivities

nominal reflectivity %	reflectivity %	finesse
99.8 ± 0.05	99.75	1255
	99.85	2093
99.95 ± 0.02	99.93	4486
	99.97	10470
99.98 ± 0.005	99.975	12565
	99.985	20942

Table 4. Cavity parameters

mirror material	ULE
mirror diameter	15 mm
mirror radius of curvature	500 mm
mirror reflectivity	99.98 %
cavity material	ULE
cavity length	90 mm
cavity finesse	15710
cavity FSR	1.67 GHz
cavity FWHM	106 kHz

2.2. Mirror radius of curvature

For ease of mode matching, and for reducing the number of higher-order modes sustained by the cavity, it is better to have a cavity waist as big as possible. Of course, we don't want a cavity with flat mirrors, which is on the boundary of the stability curve. A radius of curvature 3-4 times the cavity length should work. Figure 5 shows the dependance of the cavity waist on the mirror radius of curvature.

2.3. Oscillation of higher-order modes

Given the 15 mm mirror diameter, the cavity is not sensitive to misalignment (the spot diameter at the mirror is about 100 times smaller) [11]. It is possible that the cavity will oscillate on transverse modes other than the fundamental, because diffraction losses are small for a great number of higher-order modes. It is believed that, given the high spectral purity of the laser beam (50 kHz free-running, much less when locked), with a proper mode matching higher-order modes will not be excited.

2.4. Cavity parameters

Table 4 shows the relevant parameters of the cavity.
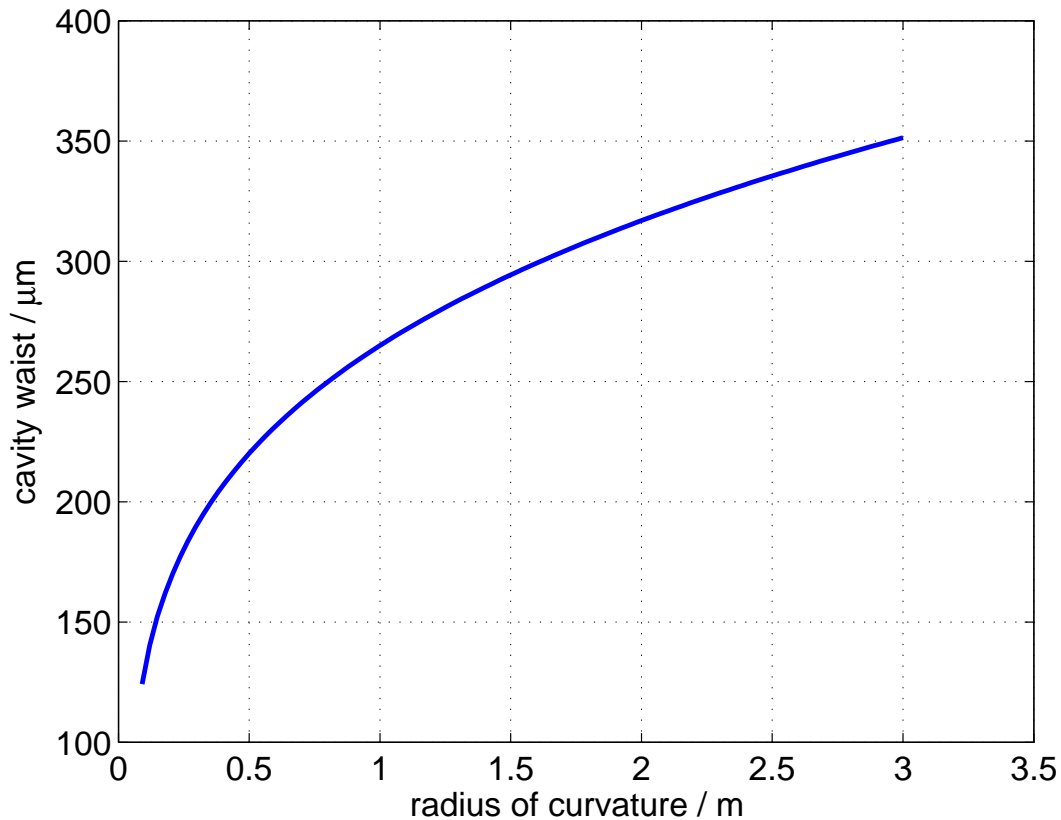
Figure 5. Cavity waist as a function of mirror radius of curvature

3. Thermal considerations and sensors placement

In our system, many sensors will be used to control the temperature of the ULE spacer; some of them can be directly connected to the vacuum system or to the shields but none can directly touch the ULE spacer in order to avoid mechanical deformations or transmit vibrations and the like.

More exactly, two temperature measurement methods were proposed. The first one employs conduction of heat between the object under observation and the sensor; this technique is to be applied to the vacuum system and to the shields.

The second measurement method should employ thermal coupling by means of the heat radiated by the ULE spacer.

As the temperature control relays on the measurement of the ULE temperature, we need to evaluate the accuracy of such a measurement.

Thus, before proceeding further, a thermal analysis of the two inner sensors (inner shield and ULE) is needed in order to assess the expected measured values and to avoid potential damages to the ULE cavity itself.

Figure 6 shows a simplified model of a generic temperature sensor and the model of heat diffusion.

The sensor model describes the expected temperature measurement when the sensor is used in the "real world", *i.e.* when subjected to self heating due to the power supply, thermal coupling to other systems because of the presence of the wires, bandwidth limitations due to thermal capacitance and non-ideal coupling with the object under measurement. Non-linearity is neglected in this analysis although it is usually present. The heat diffusion model presented in figure 6, has been reported only for reference as
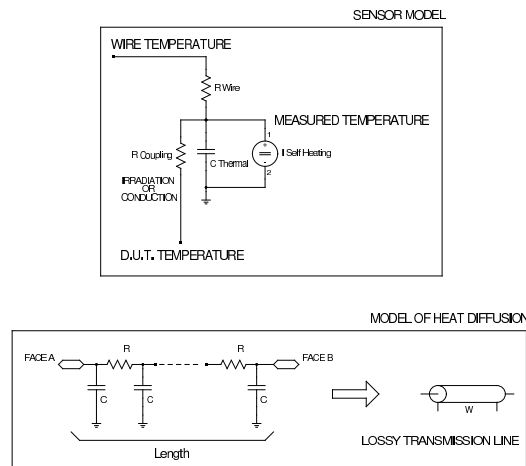
Figure 6. Thermal models of some elements

in the analysis of the system it will be neglected.

3.1. Placement of temperature sensors

Because of the geometry of our thermal system, a cylindrical coordinate system (r, ϕ, z) will be used. We will refer to r as "radial" coordinate, ϕ as "azimuthal coordinate" and z as "longitudinal coordinate".
  The analysis of the system can be separated into two directions:

- **Radial dimension**. The vacuum chamber, the thermal shields and the ULE spacer can be approximated as r-dependent elements because of the rotational symmetry around the z-axis. In the first analysis the longitudinal coordinate will be neglected because of the uniformity of the heater and the good thermal insulation at the ends (infinite length cylinder approximation). Other z discontinuities and further variations of temperature and heat flow which could occur along the z axis will be neglected now.

- **Longitudinal dimension**. As the wires are placed in the region between the shields parallel to the cylinder's axis, the behaviour of the connections between the sensors and the external connector is a longitudinal problem.

The cross-section of the vacuum system shown in figure 7 is the starting point of our model. As stated before, the wires ($W_{2-6,U}$) lay in the longitudinal dimension, thus
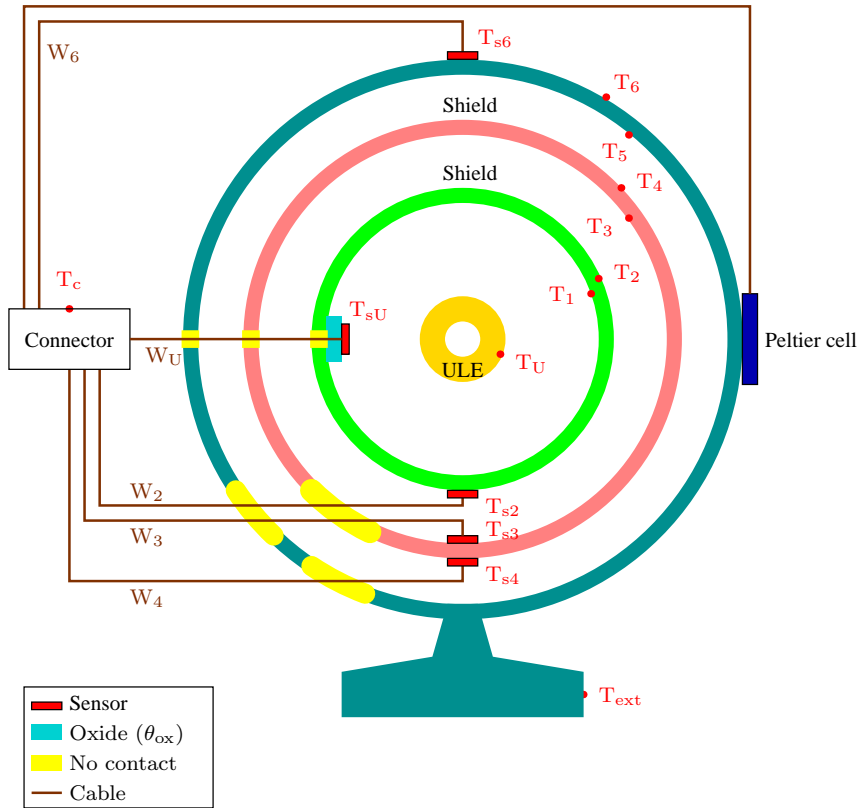
Figure 7. Vacuum system section

in our model they will be taken into account separately. Our thermal model will be constructed in two steps:

- add the *r*-dependent components found in figure 7 along the radial dimension;
- add the *z*-dependant components (wires).

The resulting model is shown in figure 8.

3.2. Simplified sensor model

Although the complete model in figure 8 can provide us with many informations, now we are not interested in the general behaviour of the whole system and thus the analysis can be greatly simplified under the following assumptions:

- the system is in stationary conditions, thermal capacitances and diffusion processes are neglected;
- the vacuum system and the first shield have no effect of the ULE temperature due to the presence of the inner shield;
- the temperature of the ULE and the inner-shield are kept stable to T_2 and T_{ULE};
- the heat exchange between the ULE spacer and the inner shield is negligible.
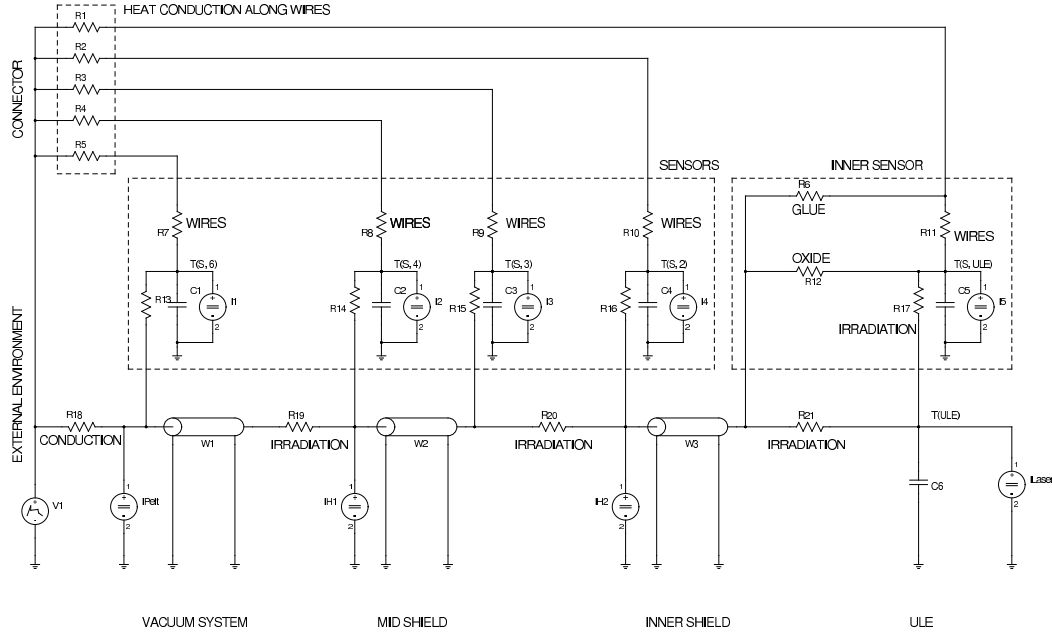
Figure 8. Thermal model

The simplified thermal model is shown in figure 9. It's worth noting that the thermal insulation between the wires of the inner sensors and the system is represented in the model by the the resistance R_6 (marked "GLUE"). Its value can either describe a "normal" insulation by means of glue or oxide, or an ideal insulation (as depicted in figure 7 by the yellow spots). The sensor itself, instead, is insulated by a suitable layer of oxide with thermal resistance R_{12}.

We now proceed in an analysis whose aim is to verify the usefulness of the inner sensor, which is supposed to measure the ULE temperature relying on radiative thermal exchange.

By simple circuit inspection, the sensed temperature dependence on the temperature of other points was calculated and reported in table 5.

Table 5. Contributions to temperature measurements of ULE spacer

Source	Temperature contribution
ULE spacer	$T_{ULE} \dfrac{1}{1 + \frac{R_{17}}{R_{12} \oplus (R_{11} + R_1 \oplus R_6)}}$
Environment	$T_{Ext} \dfrac{1}{1 + \frac{R_1}{R_6 \oplus (R_{11} + R_{12} \oplus R_{17})}} \dfrac{R_{12} \oplus R_{17}}{R_{11} + R_{12} \oplus R_{17}}$
Inner shield	$T_{Shield} \left[\dfrac{1}{1 + \frac{R_6}{R_1 \oplus (R_{11} + R_{12} \oplus R_{17})}} \dfrac{R_{12} \oplus R_{17}}{R_{11} + R_{12} \oplus R_{17}} + \dfrac{1}{1 + \frac{R_{12}}{R_{17} \oplus (R_{11} + R_1 \oplus R_6)}} \right]$
Self heating	$I_5 \cdot [R_{12} \oplus (R_{11} + R_1 \oplus R_6)]$
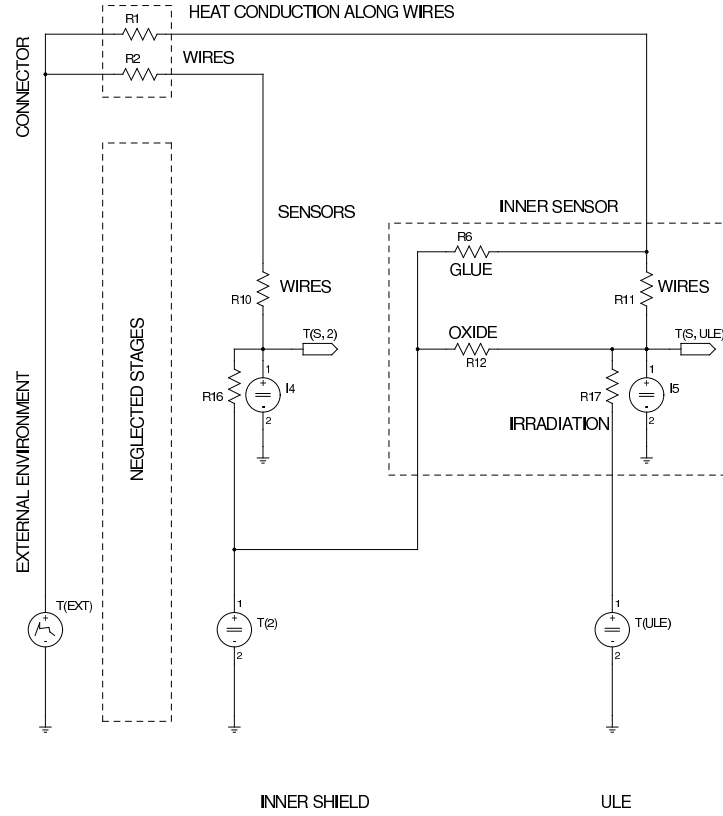
Figure 9. Simplified model

Table 6. Contributions to temperature measurements of inner sensor

Source	Temperature contribution
Environment	$T_{Ext} \cdot \frac{R_{16}}{R_2 + R_{10 and} + R_{16}}$
Inner shield	$T_{Shield} \cdot \frac{R_2 + R_{10}}{R_2 + R_{10} + R_{16}}$
Self heating	$I_4 \cdot \frac{R_{16}(R_2 + R_{10})}{R_2 + R_{10} + R_{16}}$

The heat exchange between a ULE cylinder at temperature T_{cyl} and a rectangular NTC sensor at temperature T_{rec} depends on the geometry through the view factor [12] and is given by equation (1), where $\sigma = 5.67 \cdot 10^{-8}$ W/m^2 K^4 is the Stefan-Boltzmann constant, W_{rec} is the sensor width, D is the distance between the axis of the ULE cylinder and the surface of the sensor, r_{cyl} is the radius of the cylinder and L_{cyl} the length of the radiating portion of the cylinder. The radiation efficiency η equals one.

$$P_{\text{cyl} \to \text{rec}} = 2\pi r_{\text{cyl}} L_{\text{cyl}} \eta \sigma (T_{\text{cyl}}^4 - T_{\text{rec}}^4) \frac{r_{\text{cyl}}}{W_{\text{rec}}} 2 \tan^{-1} \frac{W_{\text{rec}}}{2D} \tag{1}$$

Assuming the ULE and sensor's temperature are both close to T_0, equation (1) can be linearized, thus allowing one to compute the equivalent radiation conductance G_{irr}

$$G_{irr} = 16 T_0^3 \pi L_{\text{cyl}} r_{\text{cyl}}^2 \frac{\eta \sigma}{W_{\text{rec}}} \tan^{-1} \frac{W_{\text{rec}}}{2D} \tag{2}$$

Substituting the dimensions of our system into equation (2) and assuming $T_0 \simeq 25$ °C yields

$R_{irr} = \frac{1}{G_{irr}} \simeq 62\text{K/W}$.

As the sensor length is about 1mm, *i.e.* 1/37 of the cylinder length, the effective thermal resistance R_{17} will be approximately 37 times greater:

$$R_{17} \simeq 2300K/W \tag{3}$$

3.3. Analysis and material properties

Choosing the correct material is an important issue as the temperature measurements depend on the degree of thermal insulation and thermal match between the structures. Table 7 shows some metals' properties used to realize the wires. Two important parameters to be taken into account are the low electrical resistivity and the low thermal conductivity. Unfortunately, some material can't be used because of realization prob-

Table 7. Electrical and thermal properties of some metals [13]

Metal	Electrical Resistivity ρ_e / (Ω cm)	Specific Heat C_p / (J/g · K)	Thermal Conductivity σ_t / (W/m · K)
Copper, Cu	$1.7 \cdot 10^{-6}$	0.385	385
Silver, Ag	$1.55 \cdot 10^{-6}$	0.234	419
Aluminium, Al	$2.7 \cdot 10^{-6}$	0.9	210
Gold, Au	$2.2 \cdot 10^{-6}$	0.1323	301
Iron, Fe	$8.9 \cdot 10^{-6}$	0.44	76.2
Lead, Pb	$2.08 \cdot 10^{-5}$	0.129	33
Platinum, Pt	$1.06 \cdot 10^{-5}$	0.134	69.1
Tin, Sn	$1.15 \cdot 10^{-5}$	0.213	63.2
Titanium, Ti	$5.54 \cdot 10^{-5}$	0.528	17
Vanadium, V	$2.48 \cdot 10^{-5}$	0.502	31
Tungsten, W	$5.65 \cdot 10^{-6}$	0.134	163.3
Zinc, Zn	$5.916 \cdot 10^{-6}$	0.3898	112.2
AISI 1012 Steel	$1.74 \cdot 10^{-5}$	0.472	49.8

lems due to technological limitations. For example, although copper exhibits a higher thermal conductivity than steel, it is to be preferred because it can be welded more easily.

In table 8 some glues' thermal and electrical properties were reported. Besides the mechanical properties, not shown here, the glue used to fix the sensors' wires to the structure must exhibit a low thermal conductivity in order not to exchange heat with the substrate. On the other hand, a high conductivity glue is needed for the inner shield sensor as a good thermal match is needed.

Table 8. Electrical and thermal properties of some glues [13]

Material	Electrical Resistivity ρ_e / $(\Omega\ cm)$	Specific Heat C_p / $(J/g \cdot K)$	Thermal Conductivity σ_t / $(W/m \cdot K)$
Epoxy	10^{15}	1	0.2
Acrylonitrile	$1.9 \cdot 10^{15}$	1.3 - 1.8	0.3 - 7
Aremco-Bond 556	$9 \cdot 10^{-4}$	-	9.37

In table 9 some thermal insulators are shown. As stated about the glues, these material must exhibit a high thermal conductivity.

Table 9. Electrical and thermal properties of some insulating materials [13]

Material	Electrical Resistivity ρ_e / $(\Omega\ cm)$	Specific Heat C_p / $(J/g \cdot K)$	Thermal Conductivity σ_t / $(W/m \cdot K)$
Alumina, Al_2O_3	10^{14}	0.85	6.3
Fused Quartz	10^{14} - 10^{22}	0.7	1.4 - 2

By substitution of values from tables 8, 9 and 7, the values for the thermal resistances can be calculated, as reported in table 10.

Table 10. Thermal resistances

Type	Name	Expression/conditions	Value
Wires (Cu)	R_1, R_2	$\rho_e \frac{l}{A}$ l=10 cm, r=0.1 mm	8300 K/W
Glue (Epoxy)	R_6	$\rho_e \frac{l}{A}$ 1 mm x 1 mm x 1mm	5000 K/W
Wire-sensor	R_{11}, R_{10}	$\rho_e \frac{l}{A}$ 1 mm x 1 mm x 1mm Sn	16 K/W
Oxide (SiO_2)	R_{12}	$\rho_e \frac{l}{A}$ 2 mm x 2 mm x 2mm	360 K/W
Oxide (Al_2O_3)	R_{12}	$\rho_e \frac{l}{A}$ 2 mm x 2 mm x 2mm	80 K/W
ULE irradiation	R_{17}	equation 3 $T_{ULE} = T_{NTC} \simeq 25$ °C	2300 K/W
Shield $\rightarrow$ NTC	R_{16}	$\rho_e \frac{l}{A}$ Aremco-Bond 556 2 mm x 2 mm x 2mm	53 K/W

Substitution of the resistance values in table 10 into the temperature contributions of
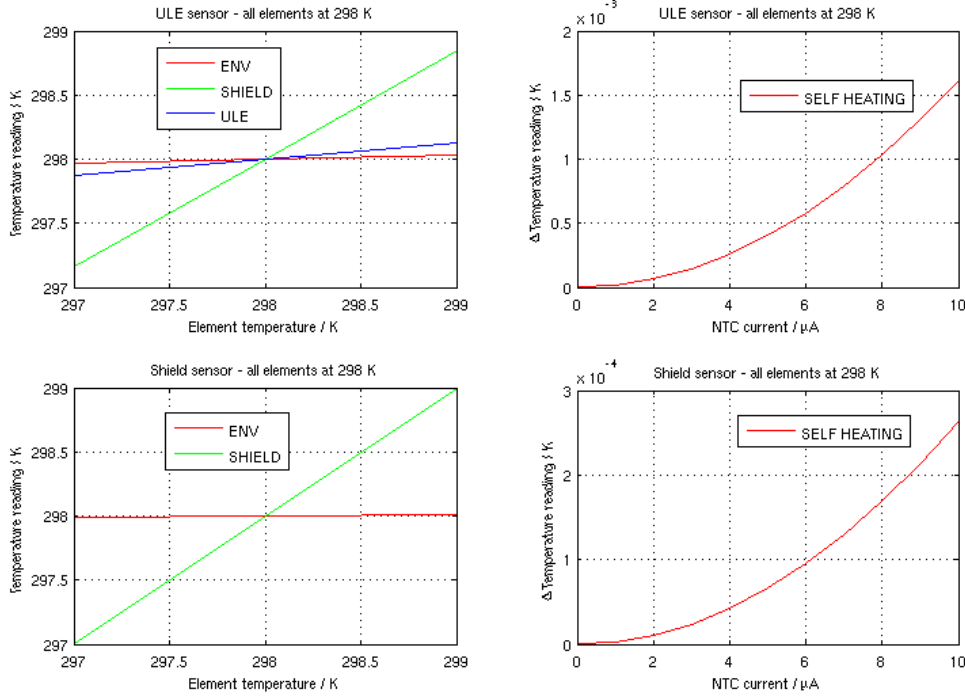
Figure 10. Sensor readings

tables 5 and 6 gives the simplified relations

$$T_{S,\,ULE} \;\; = 0.123 \cdot T_{ULE} + 0.843 \cdot T_{Shield} + 0.0339 \cdot T_{Ext} + 323\frac{K}{W} \cdot P_{SelfHeating}$$

$$T_{S,\,Shield} = 0.994 \cdot T_{Shield} + 0.00633 \cdot T_{Ext} + 53\frac{K}{W} \cdot P_{SelfHeating}$$

As shown in figure 10, the inner (glued on the inner surface of the internal shield, directly facing the ULE) sensor's readings are mainly influenced by the underlying shield temperature. Moreover, the sensor itself could be damaged during the launch, or the connecting wires could break during the launch phase and be put in contact with the ULE, resulting in a mechanical perturbation. The authors suggest that this sensor has not to be used.

4. Cavity thermal stabilization

The laser stability depends on the mechanical stability of the reference cavity. Given a target frequency stability $\frac{\delta\nu}{\nu} = 1 \times 10^{-12}$, the cavity length L must be stable to within $\frac{\delta L}{L} = |\frac{\delta\nu}{\nu}| = 1 \times 10^{-12}$. The maximum variation of the ULE's coefficient of thermal expansion (CTE) in the range 5-35 °C is $\Delta\alpha = \pm3 \times 10^{-8}$ [7]. Conservatively, the temperature of the cavity must be maintained stable to within 330 μK. The requirement can be relaxed (to a value which has to be quantified) because it is known that the CTE nulls somewhere around room temperature. The procedure to find the temperature for the minimum CTE is as follows:
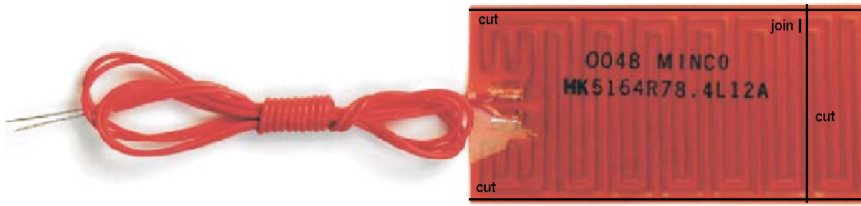
Figure 11. 25.4x50.8 mm Thermofoil heater with trimming

(i) choose an initial cavity temperature T_0 and wait for temperature stabilization

(ii) lock the laser to the cavity

(iii) slowly modulate the cavity temperature by an amount ΔT and record the correction sent by the frequency loop to the laser

(iv) repeat the above for different cavity temperatures T_i

(v) select the temperature for which the correction is null (or the smallest)

4.1. Inner shield heaters

The inner shield is composed by two parts, each 78.5 mm long and having a diameter of 46 mm. The heater choosen as a baseline is a Thermofoil from MINCO, a resistive element laminated between two insulating Kapton layers. There isn't any standard Thermofoil with the desired dimension (the closest one is the 5461/5462, 74.2x173.2 mm), so there are two possibilities: either use the standard Thermofoil - trimmed to the desired dimension, or ask MINCO to provide a custom one - a service which is offered. From Figure 11, it is clear that the Kapton layer extends 1-2 mm after the resistive element on each side, so trimming should not be a problem. In order to trim the other dimension, parts of the resisitive element must be removed, which is tricky but not impossible.

It is tempting to use a custom Thermofoil alone as the inner shield, the thermal analysis should say if it is acceptable.

4.2. Outer shield heater

The outer shield is 168 mm long with a diameter of 112 mm. There isn't any standard Thermofoil with the desired dimensions.

4.3. Temperature sensor(s)

It is the writers' opinion that one single sensor is sufficient in order to succesfully close the temperature loop.

It is unwise to increase the number of sensors: the only advantage is the measurement of the longitudinal gradient (in the hypothesis that the sensors really measure the cavity temperature, which is unlike!), if any. The price one has to pay is an increase of number

**Table 11.** EPCOS B57540G0503+00* 50 kΩ glass-encapsulated NTC thermistor

Max. power		P_{25}	18	mW
Resistance tolerance	(@ 25 °C)	$\frac{\Delta R_R}{R_R}$	2%	
Rated temperature		T_R	25	°C
Dissipation factor	(in air)	δ_{th}	approx. 0.4	mW/K
Thermal cooling time constant	(in air)	τ_c	approx. 3	s
Heat capacity		C_{th}	approx. 1.3	mJ/K

of paths through which thermal disturbances come into the controlled environment (sensor leads!)

It is possible to obtain from MINCO a Thermofoil with an integrated sensor (Pt100, Pt1000 or NTC 50 kΩ thermistor), which again is very tempting. Since the heaters are two, there would be two sensors, one for each side of the cavity.

Alternatively, a sensor can be placed somewhere, *e.g.* between the shield and the heater. Such a sensor could be, as pointed out in [14], a glass-encapsulated, NTC, 50 kΩ thermistor. Table 11 shows the characteristics of a candidate (model B57540G0503+00* from EPCOS).

Figure 12 shows a possible arrangement for placing the thermistors on the inner shield. Three longitudinal mills at 120 °C house the thermistors and their cables. The depth of the mill is slightly less than the thermistor diameter, so as to have the thermistors held in place by the heater. the non-uniformity in the shield is compensated by the heat flowing through the thermistor cables.
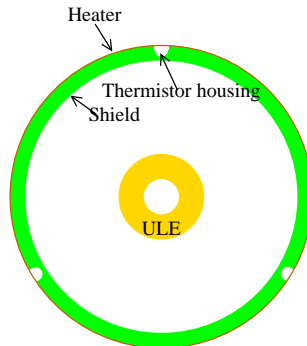
Figure 12. NTC Placement on inner shield

5. References

[1] R.W.P. Drever *et al.*, "Laser phase and frequency stabilization using an optical resonator", *Appl. Phys. B*, **31**, pp. 97-105 (1983)

[2] F. Alasia, "Relazione sulla progettazione meccanica della cavità in ULE attinente al progetto RIFERIMENTI ULTRASTABILI DI FREQUENZA OTTICA PER INTEREFEROMETRIA LASER IN APPLICAZIONI SPAZIALI", RUFO internal document

[3] E. Canuto, "Riferimenti ultrastabili di frequenza ottica. Il controllo digitale", RUFO internal document

[4] E.J. Elliffe *et al.*, "Hydroxide-catalysis bonding for stable optical systems for space", *Class. Quantum Grav.*, **22**, pp. S257-S267 (2005)

[5] http://www.rssd.esa.int/SP/SP/docs/LISASymposium/S.Rowan/Silicatebonding.pdf

[6] O. Jennrich *et al.*, "Interferometry developments for LISA and SMART-2",

[7] http://www.corning.com/semiconductoroptics/technical_information/Frame.asp?BodyURL= /semiconductoroptics/pdf/ule%5F2%5Fpage%5Fspec%5Fsheets%2Epdf

[8] A. Preston *et al.*, "Material Stability Studies for Space-Based Missions", http://www.phys.ufl.edu/~mueller/WG2/JUNE06/presentations/UFmaterial0606.ppt

[9] Michele Punturo, private communication

[10] Franck Wunderlich, private communication

[11] N. Hodgson and H. Weber, "Optical Resonators", Springer-Verlag, London, UK, 1997

[12] F. P. Incropera and D. P. DeWitt, "Fundamentals of Heat and Mass Transfer", 5th Edition, John Wiley and Sons Canada, 2001

[13] http://www.matweb.com

[14] C. Francese and G. Brida, "Bridge Circuits II", RUFO internal document, http://www.inrim.it/~brida/download.html